Template-Dependent Morphogenesis of Oriented Calcite Crystals in the Presence of Magnesium Ions

Template-Dependent Morphogenesis of Oriented Calcite Crystals in the Presence of Magnesium**

Y.-J. Han, L. M. Wysocki, M. S. Thanawala, T. Siegrist & J. Aizenberg*

Bell Laboratories, Lucent Technologies, 600 Mountain Ave., Murray Hill, NJ 07974

*To whom correspondence should be addressed. E-mail: jaizenberg@lucent.com

** We thank J. J. DeYoreo and C. Orme for constructive discussions.

Abstract

This paper presents a study of the morphogenesis of oriented crystals caused by solution growth modifiers. Self-assembled monolayers of HS-$(CH_2)_{15}$-CO_2H, HS-$(CH_2)_{10}$-CO_2H, HS-$(CH_2)_{11}$-SO_3H, HS-$(CH_2)_{11}$-OH supported on gold that induce the oriented nucleation of calcite from the (013), (113), (106)+(1.0.12) and (104) planes respectively, were used as templates for calcite crystallization from solutions containing Mg ions (Mg/Ca = 0-4). We show that when crystal growth in the presence of an additive is coupled with the control over the nucleation process, the formation of crystal arrays with extremely uniform size, shape, facets and orientation is achieved. This study for the first time demonstrates that crystal morphogenesis depends on the orientation of the crystals on the surface, such that crystals grown on different substrates exhibit uniform, but template-specific characteristics. The possible mechanisms of this new phenomenon – an additive-induced morphogenesis of differently oriented crystals – are discussed. We believe that this approach can be used as a potent crystallization strategy that would allow the synthesis of homogeneous crystals with finely-tailored morphologies.

Introduction

The ability of biological systems to exert precise control over the shape, size, orientation and hierarchical ordering of inorganic materials is of great interest to chemists and materials scientists,[1, 2] who are beginning to recognize its potential in the development of new synthetic pathways and in the improvement of existing materials. Biogenic calcium carbonate, one of the most abundant minerals formed by organisms, is a wonderful example of nature's precision.

The elaborate and unique morphologies of biogenic calcium carbonates, which in the course of evolution are cleverly refined to accommodate diverse survival functions,[1-5] have prompted extensive studies of the mechanisms of their formation.[6, 7] The development of biogenic calcium carbonates was shown to be closely associated with proteins rich in acidic/hydroxyl residues on the one hand,[1, 2, 4, 8] and with divalent cations, such as magnesium ions, on the other.[9-11] Numerous *in vitro* studies, in which calcite growth was modified by the interaction with various organic and inorganic solution additives, have reported the formation of crystals with diverse morphologies.[4, 12-20] Although these experiments were successful in demonstrating the ability to alter the morphology of calcite from its regular {104}-cleavage rhombohedron form, the modified crystals were, in general, heterogeneous in their shapes, sizes and orientations.

In particular, calcite growth in the presence of Mg ions in both synthetic and sedimentary environments was shown to result in the formation of elongated crystals that express new pseudofacets roughly parallel to the *c* crystallographic axis.[9, 13, 21-24] The habit modification was traditionally explained by face-specific mechanism involving the interaction between Mg ions and calcite surfaces parallel to the *c*-axis,[24] and recently by step-specific mechanism involving differential Mg incorporation into nonequivalent steps.[21] It has been shown that such interactions would lead to the development of calcite rhombohedra into a characteristic, elongated, roughened seed-like shape depending on the Mg/Ca ratio.[21] The experimental data showed, however, that the sizes of Mg-affected crystals, the extent of the elongation in the *c*-axis direction, the ratio between the {104} and the new, Mg-induced facets, as well as their precise {*hkl*} indices were non-uniform, even within the same experiment and using the same conditions. Here we report a new approach that makes it possible to synthesize arrays of homogeneous calcite crystals in a variety of morphological forms. In our approach, we couple the crystal growth in the presence of an additive (Mg ions) with the control over the oriented nucleation achieved by using functionalized self-assembled monolayers (SAMs) as nucleation templates.[25-27] Experiments performed with a range of template/additive combinations demonstrated the formation of arrays of calcite crystals with highly uniform sizes, shapes, orientations, composition and dynamics of growth, which are characteristic for each surface, but different for different surfaces. We discuss possible mechanisms for this intriguing new phenomenon – template-dependent crystal morphogenesis.

Results and Discussion

The four surfaces used in the experiments to control the oriented nucleation included Au films functionalized with thiols containing odd chain-length carboxylic acid (C_{15}-CO_2H), even chain-length carboxylic acid (C_{10}-CO_2H), hydroxyl (C_{11}-OH), and sulfonic acid (C_{11}-SO_3H) groups. They were chosen to correspond to the functional residues of biomolecules commonly associated with biominerals. Although ordered functional groups on surfaces alone do not mimic biomolecules, they do provide insights to the importance of ordered arrays of functional groups often displayed on the proteins that regulate the formation of biominerals.

As reported previously,[26, 27] calcite crystals grown on the surfaces of SAMs in the absence of additives were normal {104} rhombohedra that selectively nucleated from different planes induced by the SAM/metal combination. According to the X-ray diffraction and morphological analyses, more than 90% of the crystals grown from the C_{10}-CO_2H surface nucleated from the (11*l*) planes, where *l* = 3-4 (Figure 1a), and more than 95% of crystals templated by the C_{15}-CO_2H surface nucleated from the (01*l*) crystallographic planes of calcite, where *l* = 2-5 (Figure 1b). Interestingly, C_{11}-SO_3H surface provided a mixture of crystals with two dominant nucleating planes – the (106) and (1.0.12), with the ratio of 70 % : 30 % (Figure 1c). The latter observation suggests that the interfacial SO_3H groups apparently conform to two different orientations/structures upon coordinating with the Ca^{2+} ions; a possibility that is currently being investigated. More than 95 % of calcite crystals grown on the C_{11}-OH surfaces selectively nucleated from the (104) plane (Figure 1d). The sizes and nucleation densities of crystals grown on different templates are summarized in Table I.

Upon the addition of Mg ions to the solution, dramatic changes in the crystallization characteristics were observed. A small amount of Mg^{2+} ($n \leq 0.5$, n = mol Mg^{2+}/ mol Ca^{2+}) induced significant homogenization of crystal sizes, as well as of their nucleating planes for 3 acid-terminated surfaces (Table I) with no morphological changes. In the case of the sulfonic acid terminated SAMs, the addition of Mg^{2+} ($n \leq 0.5$) to the crystallizing solution favored the formation of crystals nucleating from the (106) crystallographic planes only, whereas the number of crystals nucleated from the (1.0.12) decreased dramatically. This result suggests that Mg ions are involved in the nucleation process, conceivably by promoting the preferential alignment of the -SO_3H groups at the SAM interface in the configuration, which induces the nucleation of

calcite crystals from the (106) plane, and/or by inhibiting the alternative alignment that would favor the nucleation from the (1.0.12) plane. Interestingly, upon the addition of Mg ($n \geq 0.5$), total inhibition of crystallization was observed on the C_{11}-OH surfaces, and a thin layer of amorphous calcium carbonate (ACC) spheres blanketed the surface of the SAM. This observation brings another evidence that Mg ions do not only act as the growth modifiers, but are also involved at the nucleation stage as a surface reconstruction agent, thus promoting/inhibiting the crystallization process. The formation of the ACC film is consistent with the recent studies, where proteins rich in hydroxyl residues (i.e. serine, threonine) were reported to stabilize ACC in the presence of Mg in biological systems.[10, 11, 28, 29]

A steady increase of the concentration of Mg ions beyond $n = 0.5$ further improved the uniformity of the sizes and shapes of calcite crystals (Table I). We also observed morphological changes of the regular {104} rhombohedra, with the general elongation of calcite in the *c*-axis direction (Figure 1e-k). Although for each surface type and a given *n*, the results were highly reproducible and characteristic, we detected clear differences in the morphogenesis of calcite crystals grown on C_{10}-CO_2H, C_{15}-CO_2H, and C_{11}-SO_3H. Most notably, the final modified morphologies and crystal shapes were distinctive for each surface type. In particular, progressive asymmetric development and morphological modification of Mg-affected calcites yielded arrays of uniform "dumb-bell"-shaped crystals[30, 31] on the C_{10}-CO_2H surfaces (Fig. 1e, i); arrays of uniform, tapered cylinder-shaped crystals on the C_{15}-CO_2H surfaces (Fig. 1f, j); and conically-shaped crystals on the C_{11}-SO_3H surfaces (Fig. 1g, k).

Moreover, each surface type exhibited the differences in the following parameters of the morphogenesis: (i) the ratio n_0 of Mg and Ca in the crystallizing solution, at which the appearance of the new faces was detected; (ii) the extent of the elongation in the *c*-axis direction ($r = l_c/l_{ab}$) and the ratio between the {104} and the new, Mg-induced, faces for a given *n*; (iii) the ratio n_{Mg} of Mg and Ca, at which the {104} habit disappears and the crystals exhibit only new, Mg-induced, facets; (iv) the ratio $n_{Mg,ACC}$ of Mg and Ca, at which the ACC phase starts to form and coexists with the calcite crystals; (v) the ratio n_{ACC} of Mg and Ca, at which the total inhibition of crystallization and the formation of ACC occurs. These parameters are schematically summarized in Figure 2.

Incorporation of Mg ions into the precipitates was measured by EDS and 2D shift in XRD diffraction peaks and is listed in Table I. We observed gradual increase in Mg ion

incorporation into the calcite crystals with the increase of Mg ions in the crystallizing solution. This incorporation followed nearly linear trend in the crystalline material and generally increased abruptly in the ACC phase.

Our results unequivocally show that the same growth modifier imposes different morphological changes on crystals nucleated from different organic templates, even for the same supersaturation and impurity concentration. Two mechanisms may account for this new observation. 1. The desorption of organic molecules from the SAMs would result in their cooperative interaction with the Mg ions and the growing crystals. Each surface would then produce a specific additive combination that may have a distinct effect on crystal morphogenesis. 2. The interaction between the crystal and the additive, and therefore the resulting morphology, may depend on the orientation of the crystal on the surface.

To test the first hypothesis, we carried out control experiments, in which trace amounts of one thiol were added together with Mg ions (n = 2.0) to the reaction vessel containing a substrate functionalized with the SAM of a different thiol. If the first mechanism were correct, such addition would have changed the morphology of the produced crystals (for example, from the pointed conical shape to the dumb-bell shape upon the addition of HS-$(CH_2)_{10}$-CO_2H to the solution when the SAM of HS-$(CH_2)_{11}$-SO_3H was used as a template). No apparent changes in morphologies were, however, observed.

The second hypothesis was verified in two different experiments. First, we precipitated calcium carbonate in the presence of Mg (n = 1.25) on a methyl-terminated SAM that does not induce the oriented nucleation and produces an array of randomly oriented calcite crystals. The concentration of magnesium was chosen to correspond to the interval that showed the most pronounced differences in crystal morphogenesis (see Fig. 2). We observed that the extent of the morphological modification differed significantly between differently oriented crystals, though the same organic molecule may have leaked into their vicinity. We also noticed the tendency of crystal shapes to change from conical to cylindrical, as the orientation of their *c*-axes changes from perpendicular to parallel to the substrate. This observation is consistent with the shapes of the crystals grown on the sulfonic acid-terminated surface versus carboxylic acid-terminated surface, where the angle between the *c*-axis and the SAM is ~57º and ~23º respectively. In the second experiment, calcite crystals were grown epitaxially on a biogenic calcite crystal (echinoderm skeletal elements) in the presence of Mg. The surfaces of the echinoderm crystals

are round and are, therefore, differently oriented at different locations in respect to the *c*-axis of the constituent calcite. We observed that the crystals nucleated at the surfaces roughly perpendicular to the *c*-axis are indeed conical, while the crystals nucleated at the surfaces parallel to the *c*-axis exhibit cylindrical shapes (Figure 3).

These control experiments confirm that the morphological changes induced by a growth modifier depend primarily on the orientation of the crystal on the surface. For randomly oriented crystals, the difference in the relative orientation of the crystal surfaces or steps that are specifically recognized by an additive, would cause the variation in the availability/reactivity of these sites for the interaction, as well as the difference in diffusion of an additive toward them and the variation in the concentration of an additive necessary to promote morphological changes. This effect would ultimately lead to distinct, orientation-dependent morphological changes. The same mechanism can successfully be applied to explain the observed uniformity of similarly oriented crystals. In the latter case, the availability of the interacting planes to the additive and thus the modification of crystal growth is identical for all crystals, resulting in homogeneous, characteristic changes in crystal sizes and morphologies.

Although we do not exclude the possible additional effect of the desorbed organic molecules, we believe that they play a secondary role in the observed shape changes when present in low concentration (such as in the case of SAMs). Our results suggest that the effect of the organic substrate, in addition to inducing the oriented nucleation, may include sequestering of Mg ions from the solution. The extent of complexation depends on the chemistry of the organic substrate. Such effect would be manifested in the differences in the threshold values n_0 required for the morphological changes to occur, as is observed in our experiments (see Fig. 2).

In conclusion, this paper describes a new phenomenon – template-dependent crystal morphogenesis. We show that the effect of a solution growth modifier on the crystal shapes and sizes depends on the orientation of the crystals on the surface. For a specific organic template that induces oriented nucleation of the crystals from the same plane, the resultant crystal arrays are, therefore, highly uniform in size, morphology and orientation, characteristic of the template/additive combination. We also present interesting evidence that the Mg ions are involved in the nucleation process and that the surfaces functionalized with hydroxyl groups display the capacity to stabilize the formation of amorphous calcium carbonates with little or no Mg ions present. The impressive crystal homogeneity that is achieved, when the addition of a

specific crystal growth modifier is coupled with oriented nucleation, suggests that the above approach can be used as a powerful synthetic route leading to crystalline materials with controlled properties.

Experimental

SAMs were prepared by soaking a 50nm gold film, which was E-beam evaporated on a Si(100) wafer primed with a 2-nm Ti layer, in 5mM solutions of HS-$(CH_2)_{11}$-OH, HS-$(CH_2)_{10}$-CO_2H, HS-$(CH_2)_{15}$-CO_2H, and HS-$(CH_2)_{11}$-SO_3H in alcohol for a minimum of 6 hrs.[32] Calcium carbonate precipitation on SAMs was performed as described in our previous reports, using stock solutions of $CaCl_2$ (25mM), $MgCl_2$ (25mM, 150mM), and $(NH_4)HCO_3$(s).[25, 26, 32] Experiments were carried out in a cell culture multidish containing 24 reaction vessels. Every reaction vessel was filled with 2 ml of $CaCl_2$ (25mM stock solution) with appropriate amount of $MgCl_2$ (25mM or 150 mM stock solution) and H_2O to total the volume at 4 ml. Magnesium to calcium ratios, *n* ($n = Mg^{2+}/Ca^{2+}$), were varied from 0 to 4 with an increment of 0.25. To ensure identical experimental conditions for a reliable comparison between different substrates and various *n*, crystallization was carried out simultaneously for all SAMs and 6 different *n* values in the same culture dish. The substrates were always completely submerged beneath the solution-air interface for consistency in crystallization. The crystallization took place inside a desiccator at room temperature for 2 hrs. Each substrate was then rinsed with H_2O and dried with compressed N_2. The crystals were characterized by scanning electron microscopy (SEM) with energy dispersion X-ray attachment (EDX), X-ray diffraction (XRD) using Cu Kα radiation, and computer simulation of the morphology using SHAPE6.0 program.

[1] H. A. Lowenstam, S. Weiner, *On Biomineralization*, Oxford University Press, Oxford, **1989**.

[2] S. Mann, *Biomineralization - Principles and Concepts in Bioinorganic Materials Chemistry*, Oxford University Press, Oxford, **2001**.

[3] J. Aizenberg, A. Tkachenko, S. Weiner, L. Addadi, G. Hendler, *Nature* **2001**, *412*, 819.

[4] L. Addadi, S. Weiner, *Proc. Natl. Acad. Sci. U. S. A.* **1985**, *82*, 4110.

[5] S. A. Wainwright, W. D. Biggs, J. D. Currey, J. M. Gosline, *Mechanical Design in Organisms*, John Wiley, New York, **1976**.

[6] F. C. Meldrum, *International Materials Reviews* **2003**, *48*, 187.

[7] K. J. Davis, P. M. Dove, J. J. De Yoreo, *Science* **2000**, *290*, 1134.

[8] G. Falini, S. Albeck, S. Weiner, L. Addadi, *Science* **1996**, *271*, 67.

[9] S. Raz, S. Weiner, L. Addadi, *Adv. Mater.* **2000**, *12*, 38.

[10] S. Raz, P. C. Hamilton, F. H. Wilt, S. Weiner, L. Addadi, *Adv. Funct. Mater.* **2003**, *13*, 480.

[11] J. Aizenberg, G. Lambert, S. Weiner, L. Addadi, *J. Am. Chem. Soc.* **2002**, *124*, 32.

[12] J. Aizenberg, J. Hanson, T. F. Koetzle, S. Weiner, L. Addadi, *J. Am. Chem. Soc.* **1997**, *119*, 881.

[13] S. Albeck, J. Aizenberg, L. Addadi, S. Weiner, *J. Am. Chem. Soc.* **1993**, *115*, 11691.

[14] C. A. Orme, A. Noy, A. Wierzbicki, M. T. McBride, M. Grantham, H. H. Teng, P. M. Dove, J. J. DeYoreo, *Nature* **2001**, *411*, 775.

[15] D. B. DeOliveira, R. A. Laursen, *J. Am. Chem. Soc.* **1997**, *119*, 10627.

[16] J. Donners, R. J. M. Nolte, N. Sommerdijk, *J. Am. Chem. Soc.* **2002**, *124*, 9700.

[17] M. J. Olszta, S. Gajjeraman, M. Kaufman, L. B. Gower, *Chem. Mat.* **2004**, *16*, 2355.

[18] H. Colfen, M. Antonietti, *Langmuir* **1998**, *14*, 582.

[19] G. Falini, M. Gazzano, A. Ripamonti, *Chem. Commun.* **1996**, 1037.

[20] S. H. Yu, H. Colfen, M. Antonietti, *J. Phys. Chem. B* **2003**, *107*, 7396.

[21] K. J. Davis, P. M. Dove, L. E. Wasylenki, J. J. De Yoreo, *American Mineralogist* **2004**, *89*, 714.

[22] F. Lippmann, *Sedimentary Carbonate Minerals*, Springer-Verlag, New York, **1973**.

[23] J. Paquette, R. J. Reeder, *Geology* **1990**, *18*, 1244.

[24] R. L. Folk, *Journal of Sedimentary Petrology* **1974**, *44*, 40.

[25] Y. J. Han, J. Aizenberg, *J. Am. Chem. Soc.* **2003**, *125*, 4032.

[26] Y. J. Han, J. Aizenberg, *Angew. Chem.-Int. Edit.* **2003**, *42*, 3668.

[27] J. Aizenberg, A. J. Black, G. M. Whitesides, *Nature* **1999**, *398*, 495.

[28] L. Addadi, S. Raz, S. Weiner, *Adv. Mater.* **2003**, *15*, 959.

[29] J. Aizenberg, G. Lambert, L. Addadi, S. Weiner, *Adv. Mater.* **1996**, *8*, 222.

[30] H. Colfen, L. M. Qi, *Chemistry-a European Journal* **2001**, *7*, 106.

[31] D. Kralj, J. Kontrec, L. Brecevic, G. Falini, V. Nothig-Laslo, *Chemistry-a European Journal* **2004**, *10*, 1647.

[32] J. Aizenberg, A. J. Black, G. H. Whitesides, *J. Am. Chem. Soc.* **1999**, *121*, 4500.

Table I. Crystal sizes, nucleation densities, Mg content and the extents of the elongation in the *c*-axis direction for calcite crystals grown on different SAMs in the presence of Mg

SAM	*n* = Mg/Ca	Crystal size (μm)		Elongation ratio ($r = l_c / l_{a,b}$)	Nucleation density (mm^{-2})	Mg content in calcite (mol %)
		along the *c*-axis (l_c)	in the *a,b*-plane ($l_{a,b}$)			
C_{10}-CO_2H	0	23.7±9.2		~1	1200	0
	0.5	19.3±4.1		~1	1500	6.54
	1.0	21.7±2.2	12.1±1.0	1.8±0.2	1600	8.39
	2.0	13.1±1.1	5.5±1.0	2.4±0.4	1300	8.8
C_{15}-CO_2H	0	20.6±8.0	43.8±7.2	0.5±0.2	600	0
	0.5	21.7±3.9	19.6±2.1	1.1±0.4	1900	5.96
	1.0	25.5±3.6	11.1±0.8	2.3±0.3	3200	9.21
	2.0	19.5±2.2	5.8±0.8	3.4±0.6	4400	9.21
C_{11}-SO_3H	0	$6.7±3.9_{(106)}$ $15.0±2.1_{(1.0.12)}$		~1	$10000_{(106)}$ $500_{(1.0.12)}$	0
	0.5	5.9±1.9		~1	25000	5.96
	1.0	6.3±0.6		~1	30000	7.61
	2.0	8.3±1.0	2.7±0.3	3.1±0.4	50000	8.99
C_{11}-OH	0	40.1±10.6			25	0
	1.0	$1.7±0.4_{(ACC)}$			150000	12.8

Figure Captions

Figure 1. SEM micrographs of oriented calcite crystals grown on different organic templates in the presence or absence of Mg ions. The micrographs were recorded on a JEOL JSM-5600 LV system. The SAMs and the ratios of Mg and Ca ions in solution, *n*, are indicated. a) C_{10}-CO_2H, $n = 0$. Scale bar 50 μm. Inset: Computer simulation of the {104} rhombohedron nucleated from the (113) plane. b) C_{15}-CO_2H, $n = 0$. Scale bar 50 μm. Inset: Computer simulation of the {104} rhombohedron nucleated from the (-103) plane. c) C_{11}-SO_3H, $n = 0$. Scale bar 20 μm. Crystals selectively nucleate from the (106) and (1.0.12) planes. Crystals in the (1.0.12) orientation are indicated by arrows. Insets: Computer simulation of the {104} rhombohedron nucleated from the (106) plane (left) and the (1.0.12) plane (right). d) C_{11}-OH, $n = 0$. Scale bar 100 μm. Inset: Computer simulation of the {104} rhombohedron nucleated from the (113) plane. e) C_{10}-CO_2H, $n = 1.0$. Scale bar 50 μm. Inset: High magnification of an individual crystal. Although the normal {104} cleavage planes of calcite were still clearly visible (indicated by *), the crystals develop striated facets roughly parallel to the *c*-axis with a narrow center. f) C_{15}-CO_2H, $n = 1.0$. Scale bar 50 μm. Inset: High magnification of an individual, morphologically-modified cylindrical crystal. g) C_{11}-SO_3H, $n = 1.0$. Scale bar 10 μm. Only crystals nucleated from the (106) plane remain. The crystals show no morphological changes. h) C_{11}-OH, $n = 1.0$. Total inhibition of crystallization and the formation of ACC. Scale bar 10 μm. i) C_{10}-CO_2H, $n = 2.0$. Crystals uniformly develop a dumb-bell shape. ACC spheres start to form. Scale bar 20 μm. Inset: Edge-on view showing the asymmetric orientation of the dumb-bells on the surface. j) C_{15}-CO_2H, $n = 2.0$. Crystals uniformly develop a cylindrical shape. Scale bar 10 μm. k) C_{11}-SO_3H, $n = 2.0$. Crystals uniformly develop a conical shape. Scale bar 5 μm. Inset: Edge-on view showing that the crystals form a high angle with the surface.

Figure 2. Schematic representation showing morphogenetic stages of calcite crystals as a function of *n* values for different SAMs. The range of *n* values from n_{104} to n_0 indicates the stage for which no morphological changes in calcite crystals were detected. The range from n_0 to n_{Mg} indicates the stage for which both {104} and new, Mg-affected faces coexist. The range from n_{Mg} to $n_{Mg,ACC}$ indicates the stage for which only fully developed Mg-affected crystals form. The

range from $n_{Mg,ACC}$ to n_{ACC} indicates the stage, for which ACC phase coexists with affected crystals. After n_{ACC} only ACC phase was observed.

Figure 3. Epitaxial overgrowth of synthetic calcite crystals on the surface of biogentic calcite (lateral arm plate of a brittlestar) in the presence of Mg. Note that the crystals grown from the surfaces roughly perpendicular to the *c*-axis have highly tapered, conical shape (a), while the crystals grown on the surfaces roughly parallel to the *c*-axis form cylinders (b).

Figure1

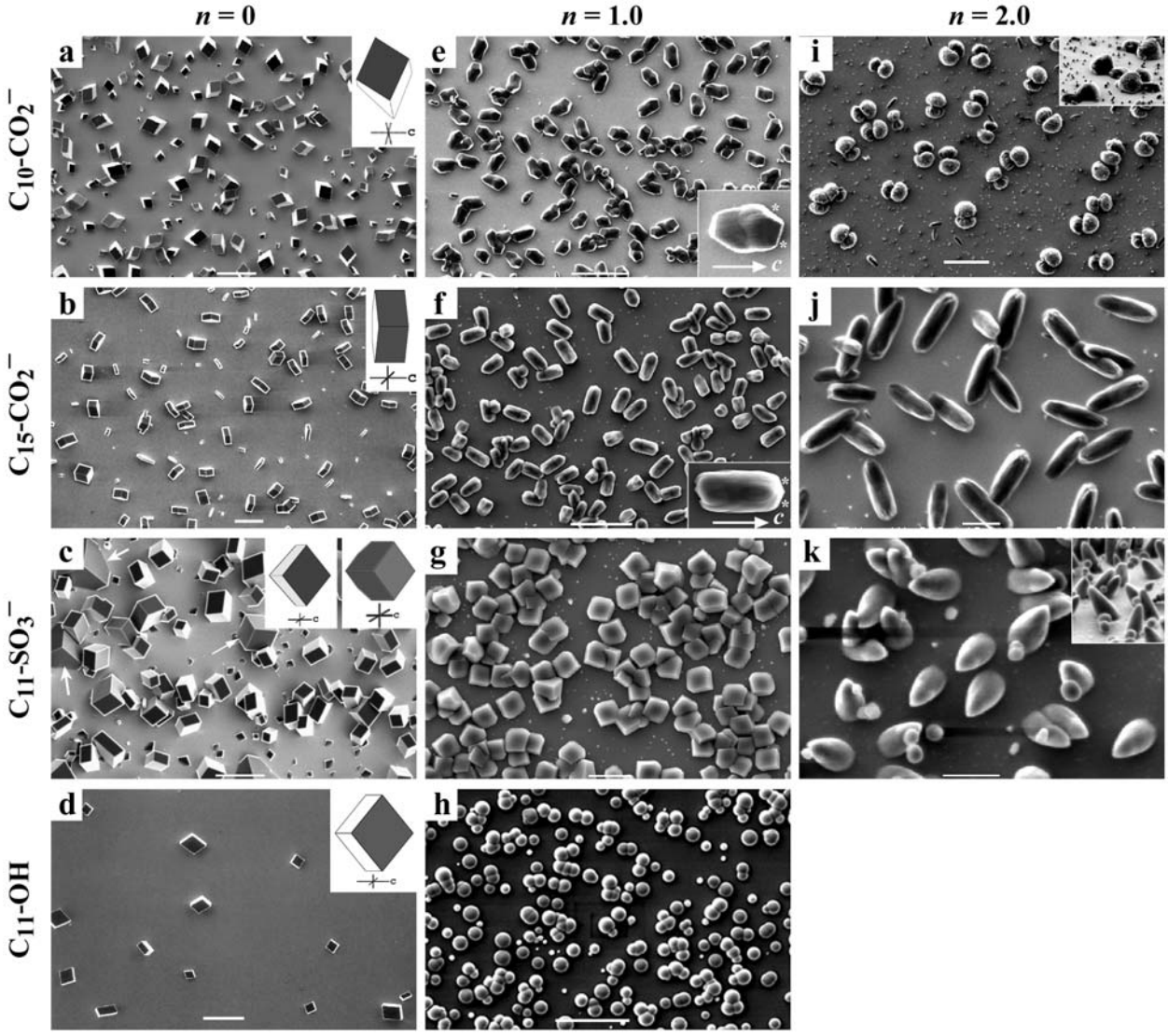

Figure 2

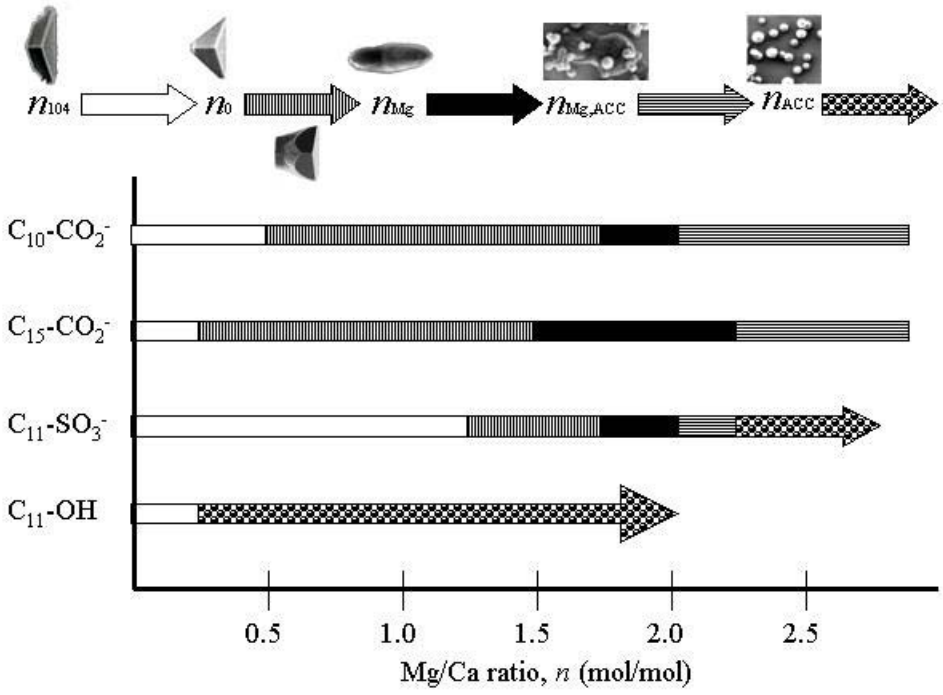
n_{104}
n_0
n_{Mg}
$n_{Mg,ACC}$
n_{ACC}
C_{10}-CO_2^-
C_{15}-CO_2^-
C_{11}-SO_3^-
C_{11}-OH
0.5
1.0
1.5
2.0
2.5
Mg/Ca ratio, n (mol/mol)

Figure 3